Available online at www.sciencedirect.com

ScienceDirect

Procedia CIRP 87 (2020) 450–455

www.elsevier.com/locate/procedia

5th CIRP CSI 2020

Influence of residual stress depth distribution on lifecycle behaviour of AISI4140

Meyer, K.[a]*, Denkena, B.[a], Breidenstein, B.[a], Abrão, A. M.[b]

[a]Institute of Production Engineering and Machine Tools, Leibniz Universität Hannover, An der Universität 2, 30823 Garbsen, Germany

[b]Departement of mechanichal engineering, Universidade Federal de Minas Gerais, Av. Antonio Carlos, 6627 – Pampulha, 31270-901, Belo Horizonte, Brazil

*Corresponding author. Tel.: +49 511 762 18269; fax: +49 511 762 5115. *E-mail address:* meyer_k@ifw.uni-hannover.de

Abstract

Surface integrity has a major influence on the fatigue behaviour of metallic components. Using deep rolling, the residual stress state can be influenced to a high degree under consideration of the contact stresses between workpiece and tool. This can be used to tailor the residual stress state to improve the fatigue and lifecycle behaviour of metallic componetens. To combine the existing knowledge about the relationship between mechanical load during deep rolling and the residual stress state and lifecycle experiments, a previously developed model is applied to quenched and tempered AISI4140 components to generate parts with similar surface residual stresses but different depth distributions. The parts are stressed using rotating bending tests and the influence of the residual stress state on the residual stress relaxation and lifespan is evaluated. The results show that it is possible to influence the residual stress state to a targeted profile by the adaption of the machining parameters. The performed deep rolling experiments result in two cases: Both parameter variations result in similar compressive surface residual residual stresses. Parameter set A (high pressure, low overlap) generates a higher residual stress penetration depth and a higher roughness, while set B (low pressure, high overlap) generates a lower penetration depth and a smoother surface. The rotating bending tests result in a higher lifetime and a lower residual stress relaxation for parameter set A.

Peer-review under responsibility of the scientific committee of the 5th CIRP CSI 2020

Keywords: Residual stress depth distribution; lifecycle behaviour; deep rolling

1. Introduction

1.1. Residual stresses and lifecycle behaviour of metallic components

Residual stresses influence the functional behaviour of machined components with regard to static and dynamic strength [1,2]. Compressive residual stresses are beneficial to the fatigue behaviour of low and medium strength steels as they retard crack initiation at the surface. Tensile residual stresses must be avoided in medium and high strength steels because they promote crack initiation and propagation. However, their influence can be neglected in low strength steels. Here, changes within the micro residual stress state due to work hardening are more relevant and can increase fatigue strength as well as fatigue life [3]. During mechanical and thermal loading, such as rotating bending tests, a residual stress relaxation occurs [4,5]. The relaxation caused by mechanical load at room temperature is divided into three phases. The first phase contains the quasistatic superposition of load and residual stresses in the first load cycles due to the exceeding of local yield strengths [6]. This first phase induces a high relaxation. Afterwards, a phase of residual stress constancy occurs. The third phase is activated by crack initiation and can be accompanied by a significant change in the residual stress state [7]. Machining and load stress induced work hardening can also influence the residual stress relaxation, especially during the first load cycles [8]. The highest load stresses occur at workpiece surface and changes between tensile and

2212-8271
Peer-review under responsibility of the scientific committee of the 5th CIRP CSI 2020
10.1016/j.procir.2020.02.064

compressive are applied with each reversion. The load stresses are superposed with the residual stresses. This mechanism can be used to estimate the experienced loads and the remaining lifespan [9]. While the above-mentioned authors explain the lifecycle behaviour based on the surface residual stresses, the residual stress distribution is reported to have an influence on the total life [6] and the position of crack initiation. A compressive residual subsurface state can shift the crack initiation point further below the surface [10,11] and therefore reduce the influence of the surface topography and stress concentration in grooves [12].

1.2. Influence of deep rolling processes on the residual stress state

To describe the material behaviour during machining, the thermomechanical load within the workpiece has to be taken into account [13]. During deep rolling, the thermal component can be neglected due to the absence of material separation mechanisms. The mechanical load of the deep rolling process can be described as a moving pressure source, which induces internal loads. These can be described using the Hertzian contact relationships. Here, a contact between two spheres can be assumed [14,15]. An influence of the maximum equivalent stress $\sigma_{eq,max}$ and the maximum residual stresses in axial σ_{II} direction has been observed by Meyer and Kämmler [14]. Using this approach, it is possible to perform a prognosis of the maximum residual stresses based on the process parameters following a set of parameterization experiments for individual workpiece materials. Because deep rolling induces plastic deformation, this approach can be discussed, because Hertz laws apply for elastic deformation. But according to the achieved results, the calculated stresses can well be used for an assumption of the mechanical load during machining. Denkena et al. extended this approach by including the overlap u, which is a unitless factor that describes the relation between workpiece material that has been in contact with the deep rolling tool and material without contact. Here an influence of said overlap could be detected with regard to the maximum residual stresses σ_{max} and their depth using quenched and tempered AISI4140 [16].

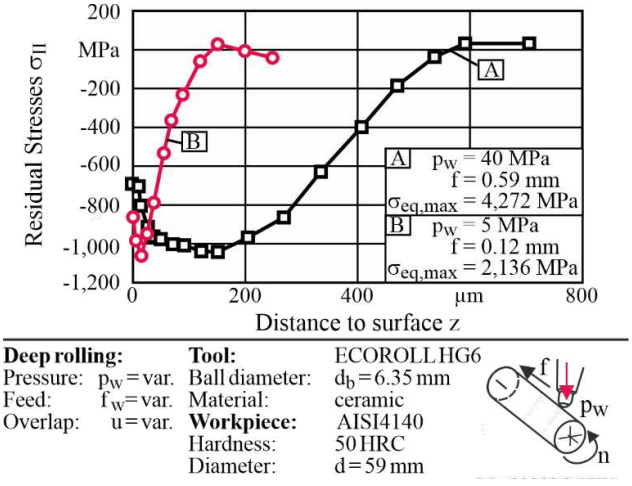

Fig. 1: Residual stress in feed direction with different profiles [16]

The above mentioned sources show that the subsurface residual stress state has a high influence on the lifecycle of periodically loaded metallic components. The deep rolling process offers the possibility to influence said residual stress state by the adjustment of the internal load. Denkena et al. showed, that it is possible to generate residual stress depth profiles with similar surface residual stresses but alternating depth distributions [16] for workpieces with a diameter of $d = 59$ mm (see Fig. 1). This paper aims to adapt the deep rolling parameters to transfer these profiles on samples with alternating diameters to perform fatigue testing. Subsequent to the machining, the samples are stressed in rotating bending tests to determine the influence of residual stress depth profiles on the residual stress relaxation and lifecycle behaviour.

Nomenclature

b	topographic peak distance [mm]
d	workpiece diameter [mm]
d_b	ball diameter [mm]
f	feed [mm]
M_{bend}	bending moment [Nm]
n	rotation speed [min^{-1}]
n_{max}	maximum rotation speed [min^{-1}]
N	number of rotations [-]
p_w	deep rolling pressure [MPa]
u	overlap [-]
λ	cut-off wavelength [mm]
σ_{II}	residual stress in feed direction [MPa]
$\sigma_{eq,max}$	maximum equivalent stresses during deep rolling [MPa]
σ_{load}	maximum load stress [MPa]

2. Experimental setup

All experiments were performed using quenched and tempered AISI4140 steel with a hardness of 50 HRC. The yield strength $R_{p0.2} = 1{,}376$ MPa is estimated according to Pavlina and van Tyne [17]. The samples were machined to the specified size according to DIN50113 (Fig. 2) using a Gildemeister CTX520 lathe with coated Sandvik DNMG150612-QM 4305 tools. The cutting speed was set to $v_c = 200$ m/min, the feed was set to $f = 0.2$ mm and a cutting depth of $a_p = 0.15$ mm was used.

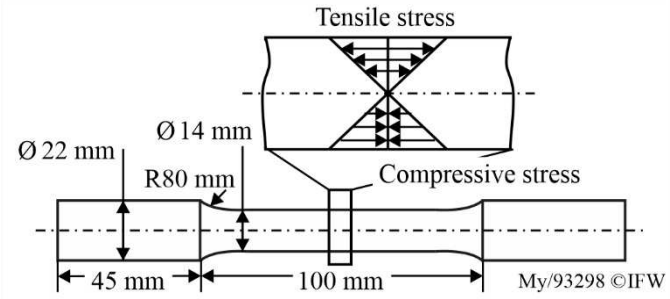

Fig. 2: Sample geometry and load stress during rotating bending tests

The subsequent deep rolling process was performed using an ECOROLL HG6 deep rolling tool with an adjustable compressor, which provides rolling pressures in a range of $p_w = 0$-55 MPa. The parameters were adjusted to induce the same maximum equivalent stresses $\sigma_{eq,max}$ and overlap u by

using Denkena et al.'s equations [16]. Table 1 shows the parameters for workpiece diameters $d = 59$ mm and the resulting adaption to the used diameter $d = 14$ mm. According to the calculation, the use $p_w = 4$ MPa to match $\sigma_{eq,max}$ for variant B is necessary. This was not possible due to inaccuracies on the compressor system for pressures near minimum level.

Table 1: Deep rolling parameters

Variant	d	f	p_w	$\sigma_{eq,max}$	u
A	59 mm	0.59 mm	40 MPa	4,272 MPa	-20 %
A	14 mm	0.48 mm	30 MPa	4,279 MPa	-20 %
B	59 mm	0.12 mm	5 MPa	2,136 MPa	50 %
B	14 mm	0.11 mm	5 MPa	2,355 MPa	50 %

The residual stresses were measured using a Seiffert XRD3000P X-Ray diffractometer using CrKα (30 kV, 35 mA) radiation using a 2 mm point collimator. Here, an accuracy of 10 MPa under ideal conditions (flat surface, small grain size, no texture) can be achieved. These conditions are not given when analyzing a workpiece with a diameter of $d = 14$ mm. Therefore, a higher uncertainty can be expected. The surface topography was analyzed using a Mahr Perthometer concept with a measurement distance of 4 mm and three repetitions. The cut-off length was set to $\lambda = 0.8$ mm according to DIN EN ISO 4287.

The rotating bending tests were performed using a Sincotec Power Rotabend test stand with a maximum bending moment of $M_{bend} = 400$ Nm and a maximum rotation speed of $n_{max} = 6{,}000$ min^{-1}. Fatigue testing was performed using 5 stress stages, which are shown in Table 2. The rotation speed was set to $n = 6{,}000$ min^{-1}. After using $M_{bend} = 110$ Nm and $M_{bend} = 135$ Nm, the step distance was reduced to 15 Nm, because of early failures.

Table 2: Bending moment M_{bend} and load stresses σ_{load} during rotating bending tests

Torque M_{bend}	Load stress σ_{load}
110 Nm	412 MPa
135 Nm	501 MPa
160 Nm	594 MPa
175 Nm	650 MPa
190 Nm	705 MPa

The samples were removed after a number of $N = 10^3$, 10^4, 10^5 and 10^6 cycles, as well as after breakage or after $N = 10^7$ cycles. Each experiment was performed thrice. This results in a total of 150 samples which were used for the fatigue experiments. During the fatigue tests, only surface near residual stresses were observed.

3. Results and discussion

3.1. Residual stress depth distribution

Fig. 3 shows the resulting residual stresses in axial direction after the internal load-based parameter adaption for parameter set A. The black line shows the target initial situation with the workpiece diameter of $d = 59$ mm. The blue line indicates the residual stress distribution for $d = 14$ mm. Both profiles have a

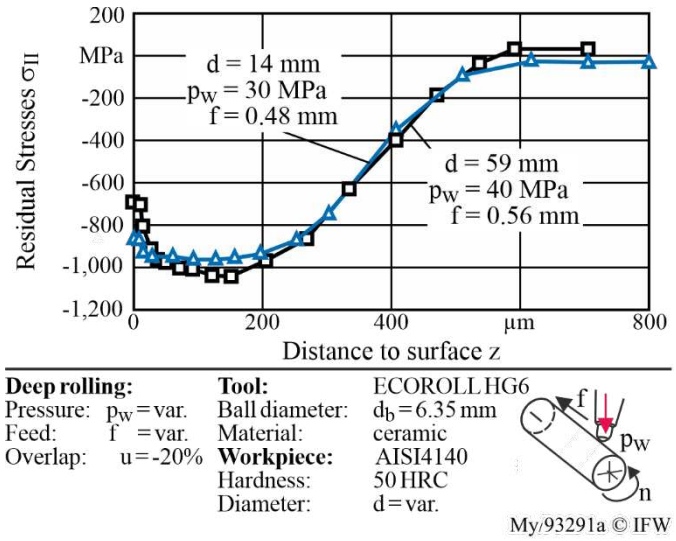

Fig. 3: Comparison of residual stress distributions for parameter set A

high similarity of measurement points below a surface distance of $z = 200$ µm. The surface near residual stresses have a higher magnitude than targeted and the residual stress maximum is in a similar depth of $z = 180$ µm. The surface near differences can be explained by the possible error of the residual stress measurement, which increases with higher surface curvatures. However, the general characteristics of the target profile are represented after the parameter adjustments. The comparison between the target and achieved residual stress profile for parameter set B is illustrated in Fig. 4.

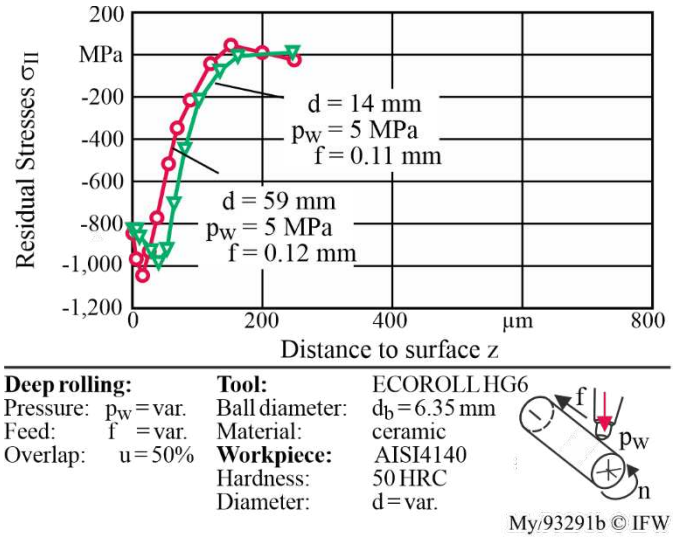

Fig. 4: Comparison of residual stress distributions for parameter set B

Here, the surface residual stresses match with a difference of below 30 MPa. The depth profile differs between both profiles in terms of the position of the maximum. This behaviour can be explained by the limited possibility to adjust the deep rolling pressure below $p_w = 5$ MPa. Therefore, a higher maximum equivalent stress $\sigma_{eq,max}$ acts on the specimen with $d = 14$ mm (see Table 1). The results from the deep rolling experiments

show that an internal load based residual stress prediction is possible after a model parametrization as performed in [16]. Using this model, it was possible to generate the desired residual stress states and create samples with similar surface residual stress states but different depth profiles for the following lifecycle experiments.

3.2. Surface topography

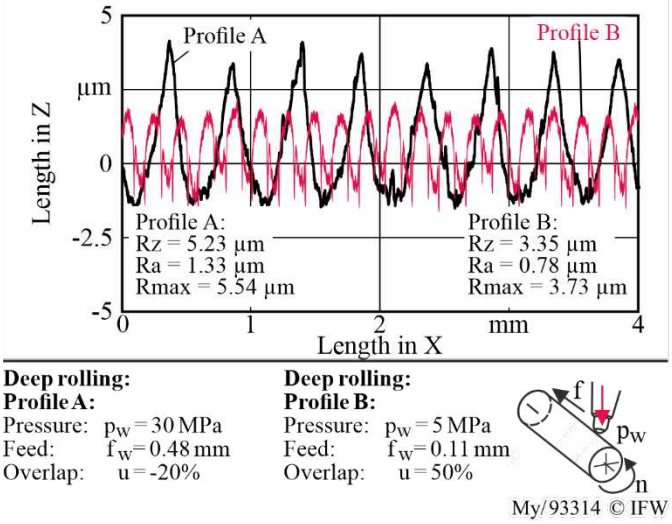

Fig. 5: Surface topography using the parameter variation

Because the surface topography plays an important role for the fatigue behaviour of metallic components, an analysis has to be performed. Fig. 5 shows the surface topography after applying the different deep rolling parameters. Using parameter set A with a relatively high deep rolling pressure of $p_w = 30$ MPa results in a full deformation of the surface. The surface contains of a periodic profile with a peak distance of $b = 0.48$ mm which results from the applied feed f. The groove geometry results from the tool radius $d_b/2$. The applied machining parameters result in a roughness of Ra = 1.33 µm, Rz = 5.23 µm and Rmax = 5.54 µm. Parameter set B with a rolling pressure of $p_w = 5$ MPa and $u = 50\%$ also induces a surface with a periodic peak distribution. Because of the comparably low deep rolling pressure, the topography contains of both, turning and deep rolling induced peaks. Here, deep rolling can be seen as the major influence, because the peak distance is $b = 0.11$ mm, which is also the feed during deep rolling. The valleys are however distorted because the mechanical load is not of sufficient magnitude for a full deformation. The machining process using parameter set B results in a roughness of Ra = 0.78 µm, Rz = 3.35 µm and Rmax = 3.73 µm. The roughness values are in a similar magnitude for both machining parameters.

3.3. Analysis of failure mechanisms

Subsequent to the deep rolling process, the samples were stressed in rotating bending tests to evaluate the influence of the deep rolling induced residual stress profiles on the lifespan and the residual stress relaxation. Fig. 6 illustrates the load stress σ_{load} dependent number of cycles until failure for both different residual stress profiles. For the lowest load of $\sigma_{load} = 412$ MPa, the samples were removed after $N = 10^7$ cycles without visible damage or breakage. Therefore, both machining variations reach the endurance range. For profile A, indicated with black square markers, the experiments with $\sigma_{load} = 501$, 594 and 650 MPa also reached the limit of $N = 10^7$ cycles.

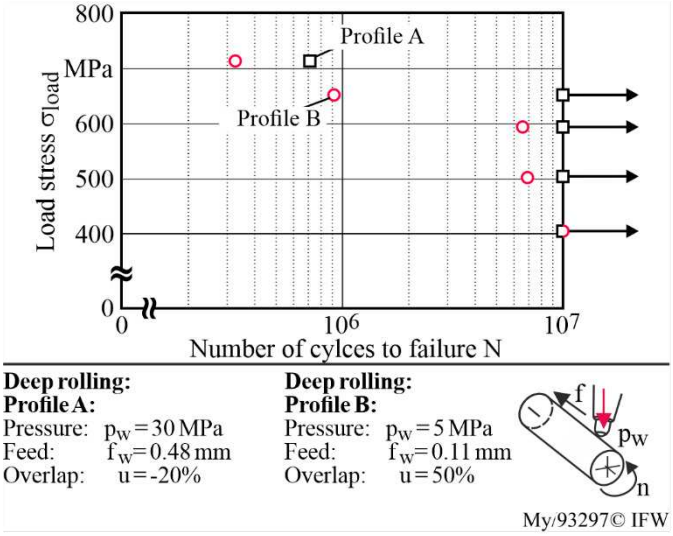

Fig. 6: Lifespan using different deep rolling parameters

Therefore, these load stresses can be categorized as endurance strength, when applying parameter set A. When using $\sigma_{load} = 705$ MPa, the lifespan is reduced to $N = 7.47\text{x}10^5$. In contrast to these results, the lifetime of the samples prepared using parameter set B decreases with increasing load stress until $n(705\text{ MPa}) = 3.35\text{x}10^5$ cycles.

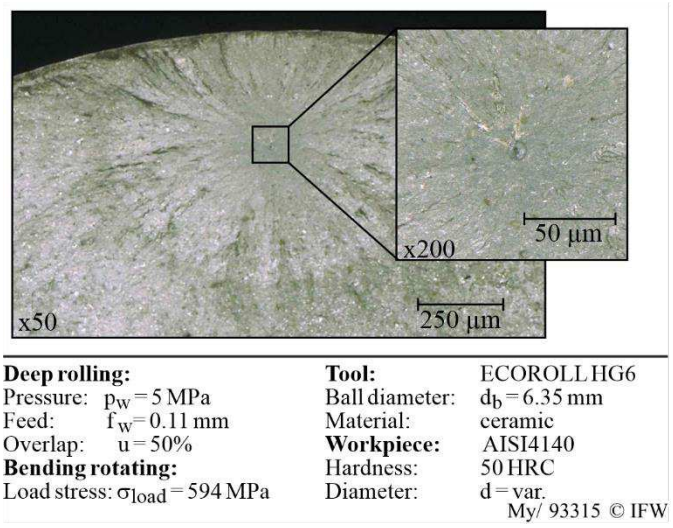

Fig. 7: Typical fractured subsurface during the experiments

The breakage mechanism plays an important role for the evaluation of the failure mechanisms and the influence of surface and subsurface properties. Fig. 7 shows a fractography of a workpiece which was machined using parameter set B and stressed with σ_{load} = 594 MPa. Here, the crack initiated below the surface. This behaviour was seen throughout all experiments with a breakage. It can therefore be concluded, that the dominant failure mechanism is not the surface topography, which can be backed by the results from Hammond and Meguid [11] and Torres and Voorwold [10]. The residual stress depth profile has an effect on the lifespan. This results also match well with the state of the art. After these experiments, it is unclear if the described behaviour also affects the relaxation and therefore the predictability of failure and estimation of experienced loads as performed by Grove and Mörke [9]. Due to the high rotation speed, it is impossible to measure the residual stress relaxation in the initial quasistatic relaxation at $N = 10^0$, 10^1 and 10^2 cycles. Therefore, the first samples were removed after $N = 10^3$ cycles. The resulting surface residual stresses during the experiments for variant A are depicted in Fig. 8. The markers are placed on the medium of three repetitions. To ensure a higher visibility, only the loads of σ_{load} = 412, 594 and 705 MPa are shown. Using the lowest load of σ_{load} = 412 MPa, only small differences in the residual stress states were measured. It can therefore be concluded, that this load is insufficient for a relaxation and the workpiece is not affected by the load. For higher loads, a significant decrease occurs between $N = 0$ and $N = 10^3$ cycles.

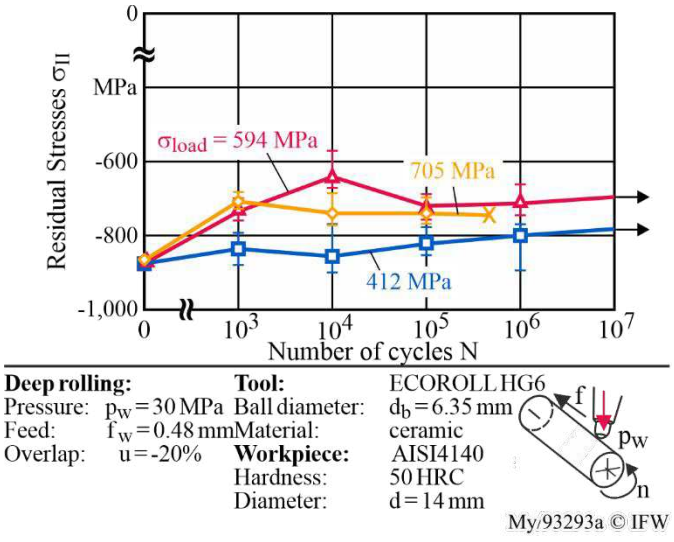

Fig. 8: Relaxation of surface near residual stresses using profile A

For higher number of cycles, no clear tendency for a residual stress relaxation can be detected. This behaviour is described in the introduction. Regardless of this residual stress alternation, all samples using the load stresses of σ_{load} = 412, 501, 594 and 650 MPa, reached $N = 10^7$ load cycles. Using σ_{load} = 705 MPa, no relaxation after the initial relaxation between $N = 0$ and $N = 10^3$ cycles can be detected. After $N = 7.73 \times 10^5$, the samples break without further indication. This behaviour stands in opposition to the sources stated in the introduction, where a drop of residual stresses indicates the upcoming material failure. One possible reason for this is the logarithmic frequency of residual stress observation. A relaxation could have occurred between $N = 10^5$ and 7.73×10^5 cycles, but was not measured. To evaluate this phenomenon, further experiments using a smaller distance in this region of interest are required.

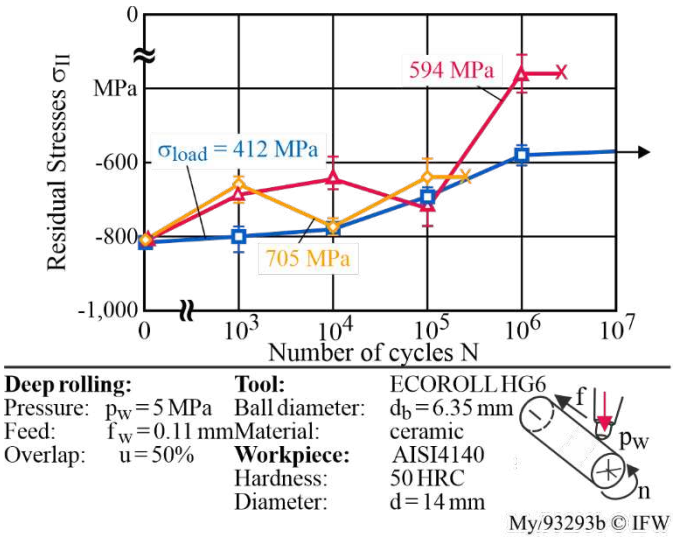

Fig. 9: Relaxation of surface near residual stresses using profile B

Fig. 9 shows the residual stress relaxation for the different applied load stresses using parameter set B. As stated previously, it was only possible to reach the endurance strength limit for a load stress of σ_{load} = 412 MPa. For this load, a residual stress relaxation occurs over the load cycles. After $N = 10^7$ cycles, a difference of $\Delta\sigma_{II}$ = 218 MPa in comparison to the initial state was measured. This relaxation is a good match to the state of the art. It is higher in comparison to the relaxation of the sample machined using parameter set A. A similar behaviour is visible for the residual stress relaxation using higher loads. Here, a significant residual stress relaxation was measured before material failure. When applying higher loads, the described phase of constancy in the residual stress between $N = 10^3$ and 10^6 cycles is visible. According to Grove and Mörke, a higher load would induce a stronger initial relaxation [9]. This reaction could not be observed with the examined components, where a similar relaxation occurred when using σ_{load} = 594 and 705 MPa. For these parameters, a significant residual stress decrease can be detected before breakage. This matches the described behaviour from the introduction. After this experimental section, it can be confirmed, that the residual stress depth distribution has an influence on lifespan as well as residual stress relaxation. To explain the differences in relaxation and lifespan between the used residual stress profiles, a holistic approach, that takes several surface integrity properties such as hardness, grain structure and surface topography into account, should be developed for future applications. A first step towards an analysis of these parameters could lie in the evaluation of Full Width at Half Maximum of the X-ray peak, which can give insight over properties such as work hardening or micro residual stresses.

4. Conclusion and outlook

The first experimental section shows that it is possible to generate specific residual stress profiles by adjusting the process parameters according to internal mechanical loads. It was proven to be possible to transfer a residual stress distributions from a sample diameter of $d = 59$ mm to $d = 14$ mm. To validate this concept, a higher number of experiments is required in future research applications. The different residual stress profiles had similar surface near stress levels, but alternating depth profiles, which were used to investigate their influence in fatigue testing. The second experimental section showed that higher residual stress penetration depth leads to a higher lifetime of rotating bending samples and a stabilization regarding the relaxation of residual stresses, which results in increased lifespan.
The lifespan was increased using a deep rolling induced higher residual stress penetration depth. The higher lifespan can be explained by a higher residual stress stability, which can be seen by less residual stress relaxation. The relaxation did not behave as expected for some parameters based on the state of the art, where an influence of the surface near residual stress is mentioned. To increase the impact of deep rolling induced residual stress- depth distributions, more possible profiles can be observed. A first step could also lie in the full obtainment of Wöhler curve to evaluate the influence of the stress profiles on higher loads. Future research should also focus on the relaxation of deeper residual stresses, which results in higher measurement times. This problem could be addressed by using energy dispersive residual stress measurement. Using this method, depth information can be gathered without or with fewer measurement steps [4].

5. Acknowledgements

The results were obtained within the project “Powertrain 2025”. The authors want to thank the Federal Ministry of Economic Affairs and Energy (BMWi) for funding this project.

6. References

[1] C. Lipson, Stress and strength of manufactured parts, McGraw-Hill, New York, 1950.
[2] R.L. Mattson, W.S. Coleman, Effect of Shot-Peening Variables and Residual Stresses on the Fatigue Life of Leaf-Spring Specimens, 1954.
[3] G. Berstein, B. Fuchsbauer, Festwalzen und schwingfestigkeit, Materialwissenschaft und Werkstofftechnik 13 (1982) 103–109.
[4] B. Breidenstein, Oberflächen und Randzonen hoch belasteter Bauteile: Habilitationsschrift, Leibniz Universität Hannover, 2011.
[5] I.S. Jawahir, E. Brinksmeier, R. M’Saoubi, D.K. Aspinwall, J.C. Outeiro, D. Meyer, D. Umbrello, A.D. Jayal, Surface integrity in material removal processes: Recent advances, CIRP Annals 60 (2011) 603–626. https://doi.org/10.1016/j.cirp.2011.05.002.
[6] M. Leitner, F. Grün, Z. Tuncali, W. Chen, Fatigue and Fracture Behavior of Induction-Hardened and Superimposed Mechanically Post-treated Steel Surface Layers, J. of Materi Eng and Perform 27 (2018) 4881–4892. https://doi.org/10.1007/s11665-018-3543-z.
[7] S. Kodama, The behavior of residual stress during fatigue stress cycles, Proceedings of the International Conference on Mechanical Behavior of Metals II, Society of Material Science, Kyoto (1972) 111–118.
[8] A. Madariaga, J.A. Esnaola, P.J. Arrazola, J. Ruiz-Hervias, P. Muñoz, K. Ostolaza, Stability of machining induced residual stresses in Inconel 718 under quasi-static loading at room temperature, Materials Science and Engineering: A 620 (2015) 129–139. https://doi.org/10.1016/j.msea.2014.09.118.
[9] T. Grove, T. Mörke, Assessment of mechanical loads based on surface integrity analysis of machined components, CIRP Annals 66 (2017) 85–88. https://doi.org/10.1016/j.cirp.2017.04.030.
[10] M.A. Torres, H.J. Voorwald, An evaluation of shot peening, residual stress and stress relaxation on the fatigue life of AISI 4340 steel, International Journal of Fatigue 24 (2002) 877–886.
[11] D.W. Hammond, S.A. Meguid, Crack Propagation in the Presence of Shot-Peening Residual Stresses, Engineering Fracture Mechanics 37 (1990) 373–387.
[12] X. Wang, S.Q. Li, Q. Yang, B.Q. Teng, Z.X. Li, Z.W. Meng, Z.Y. Zhao, Effect of Double Shot Peening on Room-Temperature Notched Fatigue Property of TC4 Titanium Alloy, MSF 817 (2015) 90–95. https://doi.org/10.4028/www.scientific.net/MSF.817.90.
[13] G. Byrne, A New Approach to the Theoretical Analysis of Surface Generation Mechanisms in Machining, CIRP Annals 41 (1992) 67–70. https://doi.org/10.1016/S0007-8506(07)61154-8.
[14] D. Meyer, J. Kämmler, Surface Integrity of AISI 4140 After Deep Rolling with Varied External and Internal Loads, Procedia CIRP 45 (2016) 363–366. https://doi.org/10.1016/j.procir.2016.02.356.
[15] E. Broszeit, Grundlagen der Schwingfestigkeitssteigerung durch Fest- und Glattwalzen, Materialwissenschaft und Werkstofftechnik 15 (1984) 416–420. https://doi.org/10.1002/mawe.19840151204.
[16] B. Denkena, T. Grove, B. Breidenstein, A. Abrão, K. Meyer, Correlation between process load and deep rolling induced residual stress profiles, Procedia CIRP 78 (2018) 161–165.
[17] E.J. Pavlina, C.J. van Tyne, Correlation of Yield Strength and Tensile Strength with Hardness for Steels, J. of Materi Eng and Perform 17 (2008) 888–893. https://doi.org/10.1007/s11665-008-9225-5.